

Original Article

Cite this article: Andersen T and Elburg MA. Open-system behaviour of detrital zircon during weathering: an example from the Palaeoproterozoic Pretoria Group, South Africa. *Geological Magazine* <https://doi.org/10.1017/S001675682100114X>

Received: 4 June 2021
Revised: 17 September 2021
Accepted: 22 September 2021


Keywords:

Zircon; U–Pb age; trace elements; radiation damage; lead loss

Author for correspondence:

Tom Andersen,
Email: tom.andersen@geo.uio.no

Open-system behaviour of detrital zircon during weathering: an example from the Palaeoproterozoic Pretoria Group, South Africa

Tom Andersen^{1,2}  and Marlina A. Elburg¹

¹Department of Geology, University of Johannesburg, PO Box 524, Auckland Park, 2006, Johannesburg, South Africa and ²Department of Geosciences, University of Oslo, PO Box 1047 Blindern, N-0316 Oslo, Norway

Abstract

Detrital zircon in six surface samples of sandstone and contact metamorphic quartzite of the Magaliesberg and Rayton formations of the Pretoria Group (depositional age *c.* 2.20–2.06 Ga) show a major age fraction at 2.35–2.20 Ga, and minor early Palaeoproterozoic – Neoproterozoic fractions. Trace-element concentrations vary widely, with Ti, Y and light rare earth elements (LREEs) spanning over three orders of magnitude. REE distribution patterns range from typical zircon patterns (LREE depletion, heavy REE enrichment, well-developed positive Ce and negative Eu anomalies) to patterns that are flat to concave downwards, with indistinct Ce and Eu anomalies. The change in REE pattern correlates with increases in alteration-sensitive parameters such as Ti concentration and (Dy/Sm) + (Dy/Nd), U–Pb discordance and content of common lead, and with a gradual washing-out of oscillatory zoning in cathodoluminescence images. U and Th concentrations also increase, but Th/U behaves erratically. Discordant zircon scatters along lead-loss lines to zero-age lower intercepts, suggesting that the isotopic and chemical variations are the results of disturbance long after deposition. The rocks sampled have been in a surface-near position (at least) since Late Cretaceous time, and exposed to deep weathering under intermittently hot and humid conditions. In this environment, even elements commonly considered as relatively insoluble could be mobilized locally, and taken up by radiation-damaged zircon. Such secondary alteration effects on U–Pb and trace elements can be expected in zircon in any ancient sedimentary rock that has been exposed to tropical–subtropical weathering, which needs to be considered when interpreting detrital zircon data.

1. Introduction

Crystalline zircon is a robust and non-reactive mineral that can survive abrasion during repeated events of erosion and transport, and whose U–Pb system can be preserved even at high-grade metamorphic conditions (e.g. Williams, 2001; Bindeman *et al.* 2018). The crystal structure of zircon will, however, suffer radiation damage from the decay of U and Th incorporated at the time of crystallization, and their radioactive decay products. Over geological time, this will cause gradual transformation of the mineral into an amorphous substance known as metamict zircon. Whereas radiation damage itself does not cause changes in chemical composition or discordance of the U–Pb isotope system, metamict zircon is mechanically weakened (e.g. Salje, 2006) and reactive when exposed to fluids, for example during diagenesis or weathering (Balan *et al.* 2001; Willner *et al.* 2003; Hay & Dempster, 2009; Pidgeon *et al.* 2013, 2019; Andersen *et al.* 2019b). When interacting with fluids, metamict zircon commonly loses radiogenic lead causing normal U–Pb discordance; in the process, the contents of common lead and non-structural elements such as titanium, light rare earth elements (REEs) and hydrogen will increase (Stern *et al.* 1966; Black, 1987; Nasdala *et al.* 2001; Belousova *et al.* 2002; Hoskin & Schaltegger, 2003). Even elements such as yttrium, uranium and thorium can be introduced during weathering of metamict zircon (Pidgeon *et al.* 2017, 2019).

The favourable properties of crystalline zircon have made U–Pb ages from detrital zircon in clastic sediments a much-used tool for provenance identification and correlation of sedimentary strata (e.g. Zimmermann, 2018). Furthermore, the trace-element signature can be used to identify the types of igneous rocks contributing material to a basin (Belousova *et al.* 2002; Griffin *et al.* 2004; Veevers & Saeed, 2007). Zircon grains whose composition has been modified during diagenesis or weathering of the host sediment are less useful for these purposes. When dating igneous or metamorphic rocks by U–Pb in zircon, grains that are influenced by secondary processes can commonly be avoided by careful selection of single grains for analysis, and altered parts of grains can be removed by mechanical or chemical abrasion (Krogh, 1982; Mattinson, 2005). In detrital zircon geochronology, the priority is to establish an unbiased estimate of the zircon population in the samples studied. This is commonly achieved by random sampling from a bulk

© The Author(s), 2021. Published by Cambridge University Press. This is an Open Access article, distributed under the terms of the Creative Commons Attribution-NonCommercial licence (<http://creativecommons.org/licenses/by-nc/4.0/>), which permits non-commercial re-use, distribution, and reproduction in any medium, provided the original article is properly cited. The written permission of Cambridge University Press must be obtained prior to any commercial use.

CAMBRIDGE
UNIVERSITY PRESS

zircon mineral separate, and selective methods used in isotope dilution–thermal ionization mass spectrometry (ID-TIMS) U–Pb geochronology are generally not applicable. For meaningful interpretations of sedimentary provenance, stratigraphic correlation or basin filling history to be extracted from detrital zircon data, it is important that no significant age fraction is overlooked and no spurious fraction added to the dataset. To preserve such ‘qualitative representativity’ (in the sense of Andersen *et al.* 2019a), it is essential that the observed age, isotopic or trace-element distributions are not modified by alteration processes after deposition, that is, that detrital zircon has behaved as a closed system. Different data filtering criteria have been suggested to exclude analyses that have been compromised by alteration processes from detrital zircon datasets, the most common of which is to remove analyses that deviate from the U–Pb concordia curve by more than a given percentage (a discordance filter). This has the disadvantage that it may also exclude grains which are discordant only due to recent lead loss, whose $^{207}\text{Pb}/^{206}\text{Pb}$ age still retains a valid memory of the age of the protosource rock, whereas it may be inefficient against bias-inducing lead loss caused by processes in the past (Andersen *et al.* 2019a). Other filtering criteria that have been proposed are based on trace-element parameters (Bell *et al.* 2019) or common lead content (Andersen *et al.* 2019b). The main concern when using such data filters should be to remove grains whose U–Pb isotope systematics have been affected, while retaining as much of the valid information in the randomly sampled dataset as possible.

The vulnerability of zircon to alteration depends on the degree of structural damage, which is related to the alpha radiation dose accumulated over the lifetime of a zircon grain. At time t , a crystal formed at $t_i > t$ will have accumulated an alpha radiation dose given by:

$$D_\alpha(t) = x_9; \frac{N_A}{10^6} \left[\frac{8A_{238}C_U}{M_{238}} (e^{\lambda_{238}t_i} - e^{\lambda_{238}t}) + \frac{7A_{235}C_U}{M_{235}} (e^{\lambda_{235}t_i} - e^{\lambda_{235}t}) + \frac{6C_{Th}}{M_{232}} (e^{\lambda_{232}t_i} - e^{\lambda_{232}t}) \right] \quad (1)$$

where A_{235} , A_{238} are the natural isotopic abundances of ^{235}U and ^{238}U ; M_{235} , M_{238} and M_{232} are the atomic masses of ^{235}U , ^{238}U and ^{232}Th ; C_{Th} and C_U are the concentrations (in parts per million) of U and Th; and N_A is the Avogadro constant. The formula was first defined for $t = 0$ by Holland & Gottfried (1955); here it is generalized as a function of t from the version given by Nasdala *et al.* (2004). The corresponding weight fraction of metamict material (f_m) in a zircon grain is given by the empirical relationship:

$$f_m = 1 - e^{-B_\alpha D_\alpha}, \quad (2)$$

in which $B_\alpha = 2.7 \times 10^{-19}$ g/ α (Zhang & Salje, 2001).

X-ray and spectroscopic studies have shown that the change from a fully crystalline to an amorphous state in zircon is a continuous transition process in which the crystal passes through a stage with crystalline ‘islands’ in a continuous, amorphous matrix, which is reached at what is known as the percolation point (Salje *et al.* 1999). A critical alpha dose of $D_\alpha \approx 3.5 \times 10^{18}$ α/g has been shown to be necessary to transform a fully crystalline zircon to this intermediate state (Salje *et al.* 1999), at which 61 weight percent of a grain will consist of metamict zircon according to Equation (2). Such zircon grains have lost much of their mechanical strength and resistance against chemical alteration; zircon with $D_\alpha > 3.5 \times 10^{18}$

α/g has been shown to be depleted in sediments relative to their source rocks (Markwitz & Kirkland, 2018). Further radiation damage will lead to complete metamictization at $D_\alpha \geq 8 \times 10^{18}$ α/g (Ewing *et al.* 2003).

As an example of the extent of radiation damage expected in ancient zircon, the distribution of D_α at the present day ($D_\alpha(0)$) expected from a suite of 2.2 Ga zircon with U and Th concentrations following the distribution patterns observed for granitic zircon by Belousova *et al.* (2002) is illustrated in Figure 1. In this example, only c. 22% of the zircon grains would be expected to contain less than 61% metamict material at the present time ($D_\alpha(0) < 3.5 \times 10^{18}$ α/g), whereas c. 50% of the grains would be completely metamict with $D_\alpha(0) \geq 8 \times 10^{18}$ α/g . A similar distribution based on data for zircon in a wider range of igneous rocks (gabbro to alkali granite) by Kirkland *et al.* (2015) gives a similar total range of D_α , but with a lower median value and hence lower accumulated alpha dose (23% with $D_\alpha(0) \geq 3.5 \times 10^{18}$ α/g , and 6% with $D_\alpha(0) \geq 8 \times 10^{18}$ α/g).

A consequence of this example is that a significant fraction of zircon grains from a 2.2 Ga granitic source rock would be unlikely to survive erosion, transport and deposition to make it into a sedimentary basin at the present time. Another consequence is that detrital zircons in old sedimentary rocks that were fully crystalline at the time of deposition may have acquired sufficient structural damage while residing in their host sedimentary rock, making their U–Pb and trace-element systems vulnerable to reaction with fluids in a near-surface weathering environment. Such damaged detrital grains may survive physically, as long as the host sediment is not eroded and recycled. However, both their U–Pb isotope composition and trace-element distributions may be modified.

To get a better understanding of the effects of post-depositional, *in situ* weathering on detrital zircon in ancient sedimentary rocks, and its consequences for detrital zircon geochronology, we have undertaken a U–Pb and trace-element study of zircon in samples of quartz arenites of the Magaliesberg and Rayton formations of the Palaeoproterozoic Pretoria Group in part of the Transvaal Basin of South Africa (Fig. 2). These rocks have remained undisturbed since deposition some time before 2.06 Ga (Zeh *et al.* 2015, 2016, 2020), but have been in a surface-near position and exposed to weathering since Late Cretaceous time (e.g. Partridge & Maud, 1987; Partridge, 1998).

2. Geological setting

The late Archaean – Palaeoproterozoic Transvaal Supergroup (Eriksson *et al.* 2006) comprises shales, sandstones, carbonate rocks and minor volcanic rocks, deposited on a basement of Archaean gneisses and supracrustal cover successions of the Kaapvaal Craton. It is preserved in three different basins, the Transvaal and Griqualand West basins of South Africa and the Kanye Basin of Botswana. Correlations between the successions in these basins as outlined by, for example, Eriksson *et al.* (2006), have been questioned from more recent geochronological data (Mapeo *et al.* 2006; Moore *et al.* 2012; Gumsley *et al.* 2017).

The Pretoria Group is the youngest part of the Transvaal Supergroup in the Transvaal Basin; a simplified, general stratigraphic column is given in Figure 2a. The Pretoria Group comprises two unconformity-bounded sequences, deposited in fault-controlled basins on the Kaapvaal Craton (Eriksson *et al.* 2006). Only the younger of the two sequences is of interest to the present study. In the Transvaal Basin, this succession started with terrestrial sedimentation (Boshhoek Formation) and andesitic

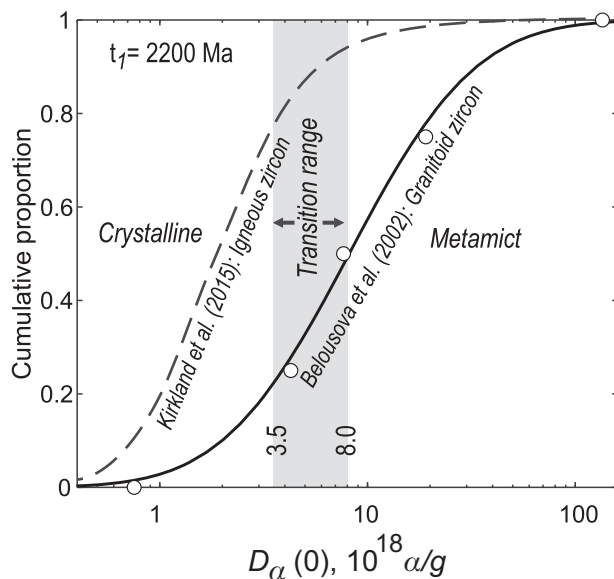


Fig. 1. Distribution of accumulated alpha dose at $t = 0$ Ma experienced by 2.2 Ga zircon with U and Th concentration distributions similar to those reported for zircon in granitic rocks by Belousova *et al.* (2002), represented by percentile points and a log-normal distribution compatible with these, and for a wider compositional range of igneous rocks by Kirkland *et al.* (2015); log-normal distribution based on data from their supplementary table A1. $D_{\alpha}(0)$ values at which zircon would have reached the percolation point (3.5×10^{18} α/g) and the complete metamictization limit (8.0×10^{18} α/g) are as given by Salje *et al.* (1999).

volcanism (Hekpoort Formation), followed by lacustrine deposition (Dwaalheuwel and Strubenkop formations), marine transgression (Daspoort and Silverton formations) and regression during deposition of the Magaliesberg Formation. The Magaliesberg Formation consists of sandstone with minor lenses of mudrock, overlying the marine shale of the Silverton Formation. It has variously been interpreted as shallow-marine, or as a succession of regression-related shore, tidal and braided delta deposits (Eriksson *et al.* 2006). The younger, 'Post-Magaliesberg' formations of the Pretoria Group are represented by the Rayton Formation in the area of this study (Fig. 2), and by several formations in the eastern part of the Transvaal Basin (Schreiber & Eriksson, 1992). These strata comprise mainly sandstones and shales, with subordinate carbonates and volcanic rocks, deposited in non-marine, probably isolated sub-basins (Eriksson *et al.* 2001). In the southern exposure area in Figure 2b, in the Potchefstroom syncline, the Magaliesberg formation occurs as discontinuous erosional remnants, and stratigraphically higher units are not preserved.

Deposition of the Pretoria Group in the Transvaal Basin must have started slightly before 2300 Ma (Hannah *et al.* 2004; Rasmussen *et al.* 2013), and terminated before eruption of the lavas of the overlying Dullstroom Formation and Rooiberg Group, the latter of which has been dated to 2061 ± 2 Ma (Walraven, 1997). Deposition was followed by emplacement of the Bushveld Complex at 2056.0 ± 0.3 Ma (Zeh *et al.* 2016) and the Vredefort meteorite impact at 2023 ± 4 Ma (Kamo *et al.* 1996). Datable units within the Pretoria Group are few, and most are only imprecisely dated (Fig. 2a), so the depositional chronology has mainly been constrained by detrital zircon data (Dorland, 2004; Schröder *et al.* 2016; Zeh *et al.* 2016, 2020; Andersen *et al.* 2019a). The succession is overlain by younger sedimentary rocks of the Palaeoproterozoic Waterberg Group of the Middelburg Basin

(Barker *et al.* 2006) and the Phanerozoic Karoo Supergroup of the Main Karoo Basin (Johnson *et al.* 2006), which are preserved as erosional remnants in the eastern part of the area of the map in Figure 2b.

The Magaliesberg and Rayton formations were deposited some time before emplacement of the Bushveld complex, of which they form the intrusion floor (Cawthorn *et al.* 2006). The age of deposition is somewhat controversial: Schröder *et al.* (2016), Beukes *et al.* (2019) and Andersen *et al.* (2019a) have suggested a maximum depositional age of *c.* 2.2 Ga for the Magaliesberg Formation, based on the youngest, major age fraction of detrital zircons observed, whereas Zeh *et al.* (2016, 2020) interpreted zircon ages as young as 2080 Ma as protosource ages unmodified by post-depositional metamorphic resetting, and therefore prefer a correspondingly younger depositional age. No detrital zircon data have been published from the Rayton Formation.

The strata of the Transvaal Supergroup have been down-warped by emplacement of the Bushveld complex, with increasing dip towards the contact. In the south, the Vredefort meteorite impact formed a series of concentric synforms and antiforms and trust sheets around the central dome, including the Potchefstroom Syncline (Fig. 2b; Brink *et al.* 1997; Therriault *et al.* 1997).

Emplacement of the Bushveld complex caused significant contact metamorphism in the Transvaal Supergroup, mainly in the floor rocks. Metamorphism locally reached anatexis grade in pelitic lithologies (Harris *et al.* 2003), and sandstones are transformed to coarse-grained, glassy quartzite in the inner part of the contact aureole (Cawthorn *et al.* 2006). Outside of the contact aureole (Fig. 2b), metamorphism is restricted to low-grade regional metamorphism in events dated to *c.* 2150 Ma and 2040 Ma (Alexandre *et al.* 2006). Thermally induced lead loss and other effects of post-depositional metamorphism in the detrital zircon would therefore be of Palaeoproterozoic age, and no younger than the age of the Vredefort impact event at *c.* 2.02 Ga.

In the northeastern part of the area shown in Figure 2, the Rayton Formation is unconformably overlain by the Wilge River Formation of the Palaeoproterozoic Waterberg Group in the Middelburg Basin, comprising red-bed sandstones and conglomerates, with minor volcanic rocks (Barker *et al.* 2006). These rocks post-date the Transvaal Supergroup, Rooiberg Group and Bushveld Complex, all of which have contributed material to conglomerates in the Middelburg Basin (Barker *et al.* 2006).

During Carboniferous–Jurassic time, southern Africa and adjoining parts of the Gondwana supercontinent were covered by sedimentary rocks of the Karoo Supergroup, followed by lavas of the Drakensberg Group. After break-up of the supercontinent, the southeastern margin of Africa remained a topographic high. By the end of the Cretaceous Period, the inland parts of southern Africa were denuded to a high-standing, gently W-sloping erosion surface bounded by a marked escarpment to the south and east (Partridge & Maud, 1987; Partridge, 1998; Partridge *et al.* 2006). In this process, the Phanerozoic cover was almost completely removed from the area of interest, so that only local relics remain; towards the east, the lower part of the Karoo succession is still intact (Fig. 2b). The erosion surface formed in this denudation cycle is partly preserved as the 'African Surface'. Regional uplift events in the Miocene and Pliocene triggered new denudation cycles represented by two younger erosion surfaces of regional importance, of which only the older 'Post African 1' surface, formed in response to Miocene uplift, is of relevance for the present study (Fig. 2b). The regional denudation history implies that the

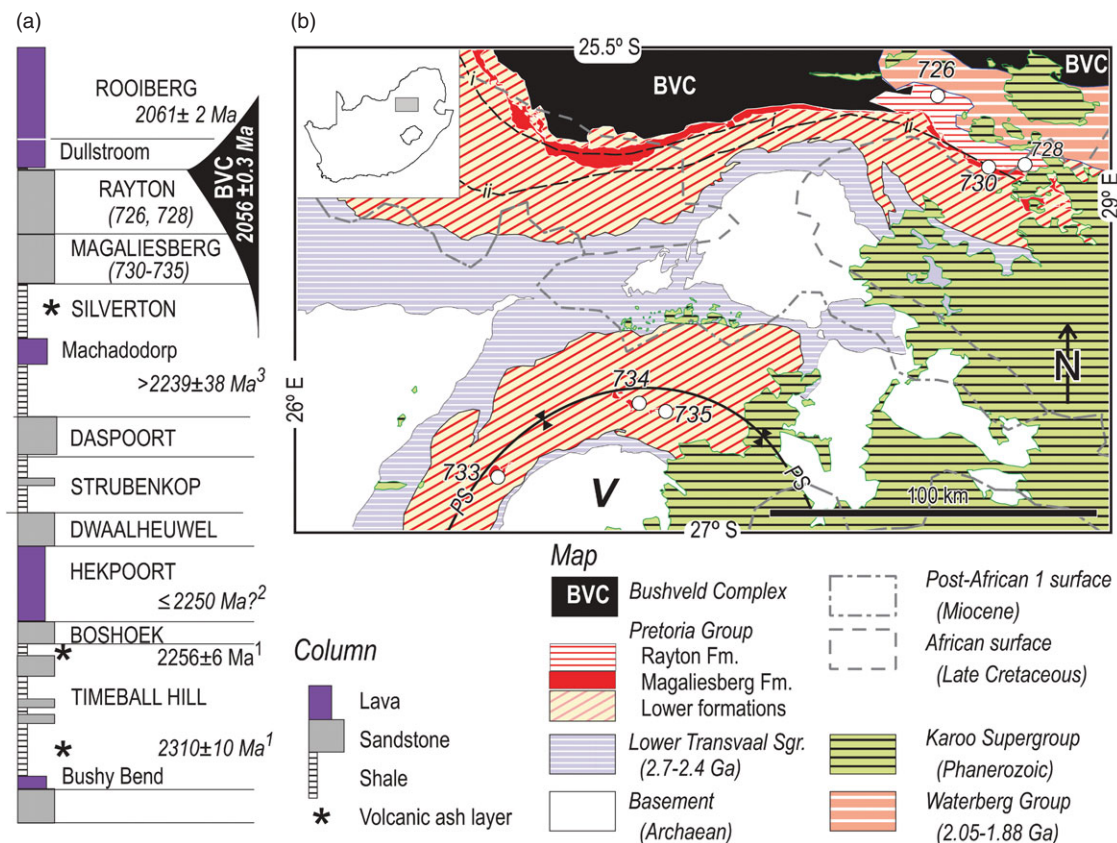


Fig. 2. (Colour online) (a) Generalized stratigraphic column of the Pretoria Group in the south-central part of the Transvaal Basin, South Africa, simplified from Eriksson *et al.* (2006, fig. 9). The Rooiberg Group lavas have been dated to 2061 ± 2 Ma by a lead evaporation age on zircon (Walraven, 1997), and the intrusive rocks of the Bushveld complex (BVC) by ID-TIMS U-Pb on zircon to 2056 ± 0.3 Ma by Zeh *et al.* (2015). Further geochronological evidence limiting time of deposition of Pretoria Group strata are: (1) Timeball Hill Formation, syn-sedimentary ashlayers, Rasmussen *et al.* (2013); (2) younger ashlayers in the Timeball Hill Formation also provide the currently most robust available maximum limit for the age of the Hekpoort lavas; and (3) minimum age of the Daspoort and lower part of the Silvertown formations sandstone is given by an Ar-Ar age on a cross-cutting mafic-ultramafic dyke swarm (Wabo *et al.* 2019). Sample numbers shown in parentheses (Magaliesberg and Rayton formations) refer to localities shown by circles in (b). (b) Simplified geological map of the south-central part of the Transvaal Basin, after Council of Geoscience 1: 250 000 geological mapsheets Rustenburg, Pretoria, West Rand and East Rand. The 500°C isograd of the Bushveld contact aureole (i) and the outer limit of the aureole (ii) are from Cawthorn *et al.* (2006). Extents of preserved African and Post African 1 surfaces are from Partridge (1998). V – Vredefort Dome, centre of the 2.02 Ga Vredefort meteorite impact; PS – axis of the Potchefstroom Syncline, from Brink *et al.* (2000).

units sampled for the present study have been in a surface-near position and exposed to weathering under variable climatic conditions for 20–70 Ma (Partridge, 1998).

3. The samples

In this study, detrital zircon has been analysed in six samples from two different exposure areas of the Pretoria Group, at different distances from the contact to the Bushveld complex (Fig. 2, Table 1). The samples were collected from roadcuts and isolated field exposures, guided by published 1:250 000 geological maps (Council for Geoscience, Pretoria). All samples were of sandstone or quartzite.

Two samples of the Rayton Formation were collected inside the limit of the contact aureole. Sample 726 is a quartzite with a distinct, pale-green colour and glassy appearance in hand specimen. Rounded detrital grains are cemented by quartz; thin rims of fine-grained chlorite around the grains are responsible for the green colour. Quartz grain boundaries are interlocking, but with sparse development of 120° triple junctions. Sample 728 is a quartz-cemented quartz-arenite. Both of the samples of the Rayton Formation contain minor ($\leq 3\%$) chert fragments. Sample 730 of the Magaliesberg Formation was collected at the limit of the

contact aureole. This sample is a partly recrystallized quartzite-quartz arenite showing graded bedding. Quartz grains are well rounded with undulose extinction and locally sutured grain contacts, with quartz cement. Samples 733, 734 and 735 come from outcrops of the Magaliesberg Formation in the central part of the Potchefstroom Syncline (Fig. 2). Sample 733 is a feldspar-free quartz arenite. Samples 734 and 735 contain up to 7% K-feldspar and minor, heavily altered lithic fragments, including chert; sample 734 also contains minor mica and apatite. All are quartz cemented, and show brown staining due to Fe-hydroxide films along grain boundaries. Zircon is a minor to accessory mineral in all of the samples (less abundant in 728 than in the other samples), occurring as well-rounded, detrital grains, without obvious post-depositional (i.e. diagenetic or metamorphic) overgrowths.

4. Methods

Samples were crushed in a steel jaw crusher, sieved to $< 250 \mu\text{m}$ using a sieve with disposable cloth. Heavy mineral separates were produced by manual washing using plastic gold-washing pans. Zircon grains were picked from these separates in alcohol under a binocular microscope, mounted on two-sided adhesive tape

Table 1. Samples analysed for the present study

Sample	Formation	Locality		S (°)	E (°)	Rock type
SA19-726	Rayton Formation	N. Cullinan	Roadcut	25.6454	28.4697	Quartzite
SA19-728	Rayton Formation	S. Bronkhorstspuit	Roadcut	25.8574	28.7389	Quartz arenite
SA19-730	Magaliesberg Formation	R25 roadcut	Roadcut	25.8651	28.6268	Quartz arenite
SA19-733	Magaliesberg Formation	SE Potchefstroom	Surface exposure	26.8215	27.1126	Quartz arenite
SA19-734	Magaliesberg Formation	SE Potchefstroom	Surface exposure	26.5937	27.5488	Subarkose
SA19-735	Magaliesberg Formation	SE Potchefstroom	Surface exposure	26.6191	27.6307	Quartzite

and cast into epoxy disks, which were ground to expose the zircon grains and polished. Care was taken to produce zircon fractions that were as non-selective as possible. The zircon mounts were imaged in cathodoluminescence (CL), using a Hitachi SU5000 field emission scanning electron microscope with a Delmic Sparc-Advanced CL System at the Department of Geoscience, University of Oslo.

U–Pb and trace elements were analysed simultaneously, using a Bruker Aurora Elite quadrupole mass spectrometer with a CETAC LS 213G2+ Nd:YAG laser microprobe, also at the Department of Geosciences, University of Oslo. Trace elements were analysed using a fast scanning protocol with dwell times as given in Table 2. NIST SRM 610 was used as calibration standard, with ^{29}Si as internal standard. Glitter software (Griffin *et al.* 2008) was used for off-line, time-resolved integration and calculation of element concentrations. Trace-element concentrations for the GJ-1 reference zircon run as an unknown are given in Table 2.

U–Pb was analysed in the same ablation runs as trace elements, with real-time integration and calibration using in-house software based on Microsoft Excel. Natural zircon reference samples GJ-1 (600.5 ± 0.4 Ma, Schaltegger *et al.* 2015), 91500 (1065 ± 1 Ma, Wiedenbeck *et al.* 1995), A382 (1875 ± 2 Ma, Huhma *et al.* 2012) and OGC (also called OG1; 3465.4 ± 0.6 Ma, Stern *et al.* 2009) were used for standardization, and the U/Pb ratio was internally standardized by $^{91}\text{Zr}/^{29}\text{Si}$. ^{235}U used for geochronology was calculated from ^{238}U , assuming $^{238}\text{U}/^{235}\text{U} = 138.77$ (e.g. Ludwig, 2012). Raw data were reduced using an interactive spreadsheet program written in Visual Basic for Microsoft Excel. Common lead was estimated from Hg-corrected measurement of ^{204}Pb , using a common lead composition given by the Stacey & Kramers (1975) model at the observed $^{206}\text{Pb}/^{238}\text{U}$ age of the zircon. Discordance is calculated from isotopic ratios rather than from ages (Guitreau & Blichert-Toft, 2014; Andersen *et al.* 2019a). Note that discordance values calculated by the two methods are neither identical nor linearly related.

Thirty-one analyses of an in-house reference zircon (A44, Kapinsalmi tonalite, Finland, ID-TIMS U–Pb age 2719 ± 4 Ma, Heilimo *et al.* 2007) gave a weighted average $^{207}\text{Pb}/^{206}\text{Pb}$ age of 2723 ± 4 Ma (95% confidence, MSWD = 1.5).

A complete listing of U–Pb and trace-element data is given in the online Supplementary Table S1 (available at <http://journals.cambridge.org/geo>).

5. Results

5.a. Zircon petrography

Cathodoluminescence images of a selection of zircon grains are shown in Figures 3–5 to illustrate the range of variation observed

in the samples studied. Detrital zircon grains are rounded, short-prismatic to elongated grains, and grain fragments. Many of the grain fragments show rounded edges cross-cutting the internal zoning pattern of the zircon, indicating that they have been abraded after breaking up (e.g. 733-67 in Fig. 4), showing that the fragmentation happened prior to final deposition. However, there are also grain fragments cut by sharp edges, which were most likely broken during crushing (e.g. grain 730-47 in Fig. 3). No systematic relationship between grain morphology or internal zoning pattern and grain size was observed, but any such relationship may have been obscured by fragmentation of the larger grains.

The internal CL structure ranges from short-wavelength–low-amplitude oscillatory zoning (730-53 in Fig. 3; 733-67, 733-93 in Fig. 4; 726-08, 728-08 in Fig. 5), typical of unmodified igneous zircon (Corfu *et al.* 2003), to uniformly CL-dark with only ghost-like CL-brighter inner zones (733-97 in Fig. 4; 728-15 in Fig. 5), suggesting post-crystallization modification that can be related to metamorphism in the protosource or in sedimentary precursors, or to processes after deposition. Between these extremes, there are grains showing more irregular, oscillatory zoning (730-47 in Fig. 3; 733-61 in Fig. 4; 728-25 in Fig. 5), probably still a primary feature of the zircon grain; grains with oscillatory zoning whose contrast has been enhanced, in that CL-dark zones have become darker and apparently also broader (730-47 in Fig. 3; 733-01 in Fig. 4; 728-10 and 728-31 in Fig. 5); and grains with completely irregular internal variations (730-46 in Fig. 3). CL-bright domains overprinting the oscillatory zoned zircon are relatively rare (730-52 in Fig. 3), and there is no evidence of growth of new zircon that can be attributed to diagenesis metamorphism of the host sediment. These observations apply to zircon in both Magaliesberg and Rayton formations, regardless of the degree of recrystallization of the host rock.

5.b. Trace-element distributions: Ti, Y, REE, Hf, U and Th

Chondrite-normalized REE patterns are illustrated for the grains shown as examples in Figures 3–5. These suggest a connection between REE distribution and CL structure, in the sense that REE patterns typical for unaltered magmatic zircon (low LREE, continuously increasing patterns towards Yb and Lu, positive Ce anomaly and negative Eu anomaly; Belousova *et al.* 2002; Hoskin & Schaltegger, 2003) are restricted to grains that show reasonably well preserved oscillatory zoning patterns. The levels of light and middle REEs increase with increasing disturbance of the CL zoning pattern and, in grains with the most severely modified structure in CL images, the REE patterns are nearly flat in the middle to heavy REE range. These grains can show concentrations above 10^4 chondrites for the most extreme cases, and some grains even show a broad maximum in the range of Sm to Dy. These

Table 2. Trace-element analyses of the GJ-1 reference zircon

Element	Isotope	Dwell time (ms)	GJ-1 (yellow)			Published	
			Mean	2SD	<i>n</i>	Zhao <i>et al.</i> (2016)	Piazolo <i>et al.</i> (2017)
Ti	49	2	5	6	176	4.63	3.35
Y	89	2	350	58	193	207	238
La	139	10	0.02	0.04	137	1.2	0.003
Ce	140	2	20	2	193	16.0	15
Pr	141	10	0.04	0.02	216	0.2	0.03
Nd	146	10	0.9	0.2	216	0.7	0.6
Sm	147	10	2.3	0.5	216	1.2	1.4
Eu	153	10	1.5	0.3	216	0.9	1.0
Gd	157	2	11	2	216	5.7	6.6
Tb	159	2	2.9	0.5	216	1.7	1.88
Dy	163	2	30	5	216	16.9	20
Ho	165	2	9.8	1.6	216	5.8	6.7
Er	166	2	43	7	216	24.9	28.7
Tm	169	2	9.1	1.4	216	5.3	6.4
Yb	172	2	86	13	216	53.9	64.8
Lu	175	2	17	2	216	10.9	11.52
Hf	178	2	8374	940	216	6538	6681
Pb	204	20	0.004	0.010	151		
Pb	206	20	25	3	151		
Pb	207	30	1.53	0.19	151		
Pb	208	10	0.29	0.06	151		
Pb	Total		28	4	216	6.6	25.3
Th	232	10	14	3	216	10	10
U	238	10	320	43	216	255	284

features are representative of the whole set of analysed grains, as is more conveniently illustrated in element versus element plots of the pooled dataset shown in Figure 6.

Titanium has a range of concentrations from near the detection limit at *c.* 2 to 4890 ppm. Y and REE concentrations are positively correlated with Ti (Fig. 6a, b), with the largest relative variation (over 4–5 orders of magnitude) for Nd and Pr (La falls under the detection limit for some grains). Th and U are also positively correlated with Ti, whereas Hf remains close to 1.5×10^4 ppm over the whole range of Ti (Fig. 6c). Because of the increasing trend in heavy REEs, the Lu/Hf ratio also increases with increasing Ti (Fig. 6d). In contrast, the chondrite-normalized Yb/Sm and Yb/Dy ratios decrease with increasing Ti, approaching or falling below 1.0 at high Ti. This reflects the tendency towards flat patterns in the middle to heavy REEs seen in some of the examples in Figures 3–5; patterns with $(Yb/Dy)_{CH} < 1.0$ have a maximum in the Dy-range. ^{204}Pb ranges from below detection limit (< 0.1 ppm) to *c.* 10 ppm, and is positively correlated with Ti, although less so than the REE (Fig. 6e). The Th/U ratio varies from 0.16 to 4.7, with a huge majority of grains having ratios between 0.3 and 3, generally increasing with increasing concentrations (Fig. 7). This is a range in which compositions of igneous and metamorphic zircon overlap (Kirkland *et al.* 2015; Yakymchuk *et al.* 2018).

5.c. U–Pb systematics

The unfiltered, common-lead-corrected U–Pb data show a range from mildly inversely discordant to almost 100% normally discordant (Fig. 6f). The discordant grains spread widely in the concordia diagram, but with a concentration of points along a lead-loss line from *c.* 2200 Ma to zero (Fig. 8a). Analyses that show a ^{204}Pb signal above the background level defined by common-lead-free reference zircons have been corrected for common lead using an average crustal lead composition according to Stacey & Kramers (1975) at the $^{206}Pb/^{238}U$ age of the zircon. This composition may not be optimal for correction for unsupported lead in zircon, causing bias towards low ages at corrections for more than 0.2–0.5% common ^{206}Pb (Andersen *et al.* 2019a). The cumulative age distribution (Fig. 8b) of the unfiltered, common-lead-corrected dataset (297 grains) shows minimum ages of *c.* 2000 Ma, and a continuously increasing trend towards older, early Palaeoproterozoic and Archaean ages, with a poorly defined age fraction in the 2200–2400 Ma range. Some highly discordant grains with $^{206}Pb/^{204}Pb$ ratios below 100 give spurious ages above 4 Ga (online Supplementary Table S1); these are completely dominated by common lead that cannot be adequately corrected for, and carry no age significance. Excluding data more than 10% discordant

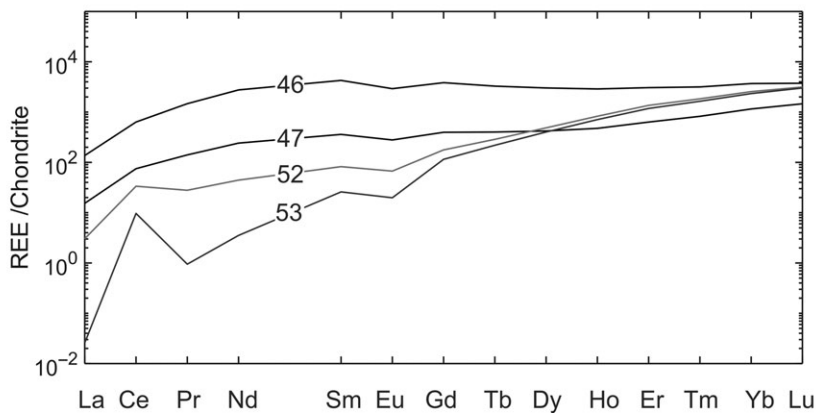
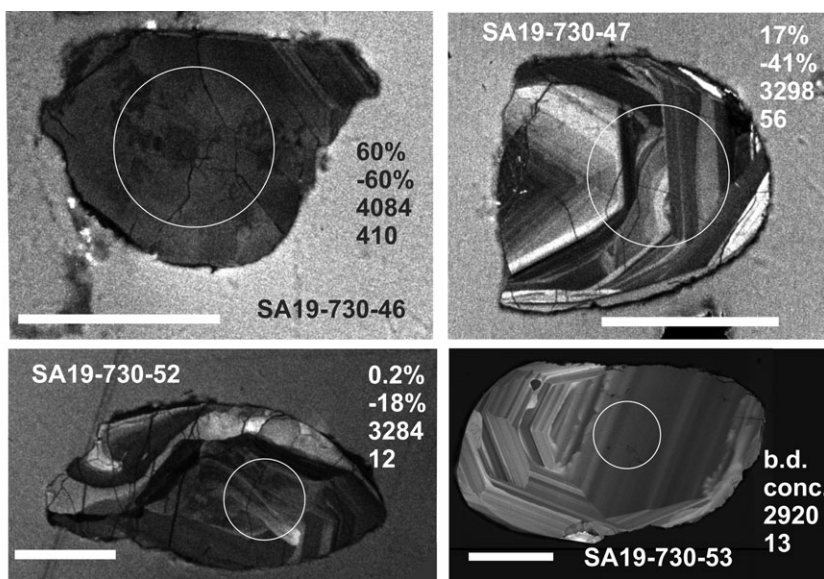


Fig. 3. CL photomicrographs of selected zircon grains from sample SA19-730, with chondrite-normalized REE patterns. Top to bottom: percentage of common ^{206}Pb (bd – below detection limit), percent discordance (or conc., which indicates that the grain is concordant within error), $^{207}\text{Pb}/^{206}\text{Pb}$ age after common lead correction, if any, in Ma, and concentration of Ti, in parts per million. Length of scale bars: 50 μm . These conventions also apply to Figures 4 and 5. Chondrite values used for normalization in this and other diagrams are from Boynton (1984).

reduces the useful dataset to 78 grains, with a major age fraction in the range 2200–2400 Ma and a smaller, late Mesoarchaeon fraction at 2900–2950 Ma. A ‘tail’ of young ages between 2000 Ma and 2200 Ma persists. These apparently young grains have been corrected for common lead, and their $^{207}\text{Pb}/^{206}\text{Pb}$ ages are most likely affected by bias due to common-lead correction (cf. Andersen *et al.* 2019a). Using $^{206}\text{Pb}/^{204}\text{Pb} > 2000$ as a limit instead of discordance (Andersen *et al.* 2019b) reduces the dataset further, to 47 useful analyses. The width of the main age fraction is reduced to 2225–2350 Ma, and a second Neoproterozoic fraction at 2750–2800 Ma is indicated. The ‘tail’ of ages < 2200 Ma disappears.

The relationship between $^{207}\text{Pb}/^{206}\text{Pb}$ age and U concentration is illustrated in Figure 9a, compared with 0, 25, 50, 75 and 100 percentiles in the granitic zircon data of Belousova *et al.* (2002), and to critical limits of present-day D_α as a function of zircon age at 3.5×10^{-19} α/g and 8.0×10^{-19} α/g . All but six of the analysed grains plot below the 75 percentile of the concentration range of granitic zircon, but a very significant proportion will still have $D_\alpha > 3.5 \times 10^{-19}$ α/g , indicating that they will be significantly radiation damaged. This can be further illustrated by the cumulative distribution of $D_\alpha(0)$ (Fig. 9b), which suggests that 68% of the zircon grains have passed the percolation limit and 39% are completely metamict. The figure also shows that the structural damage due to U and its radioactive daughters exceeds that of Th and its daughters by an order of magnitude.

6. Discussion

Detrital zircon in the samples of Magaliesberg and Rayton formations analysed in this study has suffered structural damage and disturbance to the U–Pb isotope system. Zircon of this state of preservation has limited geochronological value, and the only observations of that kind to be made with any confidence from the dataset is that the overall age distribution pattern resembles those previously reported from the Pretoria Group (Schröder *et al.* 2016; Zeh *et al.* 2016, 2020; Andersen *et al.* 2019a; Beukes *et al.* 2019). Dating of deposition or provenance identification are not the concern of this study, however. The observation that grains younger than 2200 Ma are removed by the common-lead-based data filter (Section 5.c) suggests that apparent $^{207}\text{Pb}/^{206}\text{Pb}$ ages less than 2200 Ma reflect bias induced by common lead correction (Andersen *et al.* 2019a) rather than a Palaeoproterozoic metamorphic overprint.

6.a. Primary and secondary features of the detrital zircon

Elevated Ti concentration is a characteristic feature of altered zircon (Belousova *et al.* 2002; Bell *et al.* 2019). In the present samples, the Ti concentration varies over almost 5000 ppm. The primary concentration of Ti in magmatic zircon is a function of temperature and TiO_2 activity (Watson *et al.* 2006), and the maximum

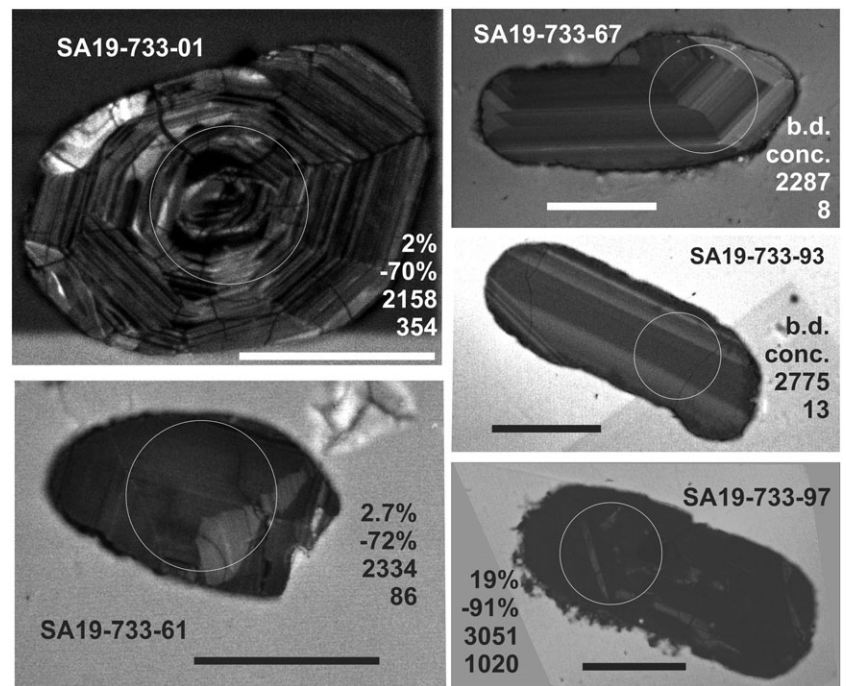
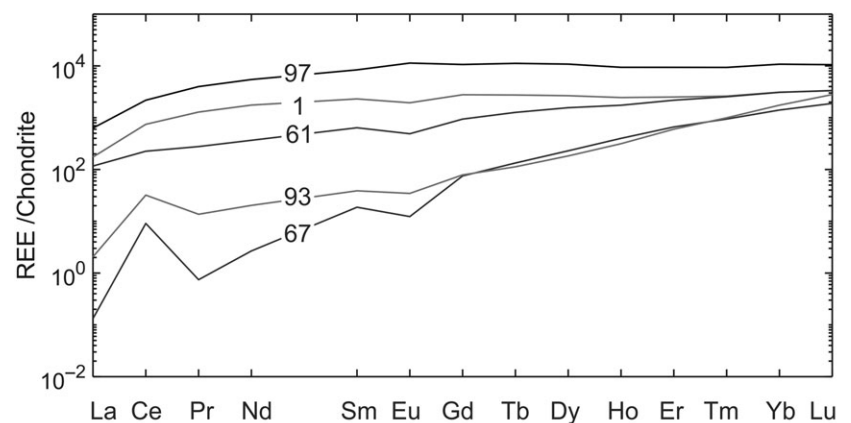


Fig. 4. CL photomicrographs of selected zircon grains from sample SA19-733, with chondrite-normalized REE patterns. See Figure 3 for abbreviations.



temperatures calculated from the observed Ti concentrations would be of the order of 2000°C, which is clearly unrealistic for zircon-fertile, felsic magmatic protosource rock. This indicates that the variation in Ti is indeed due to alteration rather than to primary differentiation in the protosource(s) of detrital zircon. The lack of correlation between Ti and Hf (Fig. 6c) indicates that the Hf concentration even in heavily altered zircon has not been affected. This suggests that the Hf concentration is a feature inherited from the protosource, perhaps the only parameter analysed in this study that is preserved in the most heavily altered detrital zircon grains in these samples.

In studies of the trace-element chemistry of ancient detrital zircon in the Jack Hills conglomerate, and suites of magmatic zircon from granites of different ages, Bell *et al.* (2016, 2019) found that the sum of un-normalized ratios $(Dy/Sm) + (Dy/Nd)$ (their LREE-I parameter) was a convenient index to distinguish primary magmatic zircon from zircon that has undergone fluid-induced alteration. Zircon with low values typically shows other evidence

of secondary disturbance (high Ti, Fe, Mn, Th/U). A distinct change of slope in plots of 'foreign' elements versus $(Dy/Sm) + (Dy/Nd)$ in their data at *c.* 50 suggested that this could be a useful limit between zircon grains that have retained their primary composition and those that have been significantly modified after crystallization. For the zircons in our study, trends in plots of, for example, U and Ti versus $(Dy/Sm) + (Dy/Nd)$ (Fig. 10a) show a change in slope similar to that observed by Bell *et al.* (2019), but at a much lower $(Dy/Sm) + (Dy/Nd)$ value (at *c.* 8, Fig. 10a), for reasons that may be related to differences in conditions (temperature, composition of fluid) or extent of alteration between the two studies. The turnover value of 8 corresponds to maximum concentrations of *c.* 300 ppm U and 40 ppm Ti (yielding a Ti-in-zircon temperature of *c.* 900°C), but with quite considerable overlap between the altered and unaltered groups, especially for U. Again, Hf concentrations show no systematic variation with $(Dy/Sm) + (Dy/Nd)$.

The Th/U ratio shows a more complex behaviour. A large proportion of grains have Th/U between 0.3 and 1, regardless of

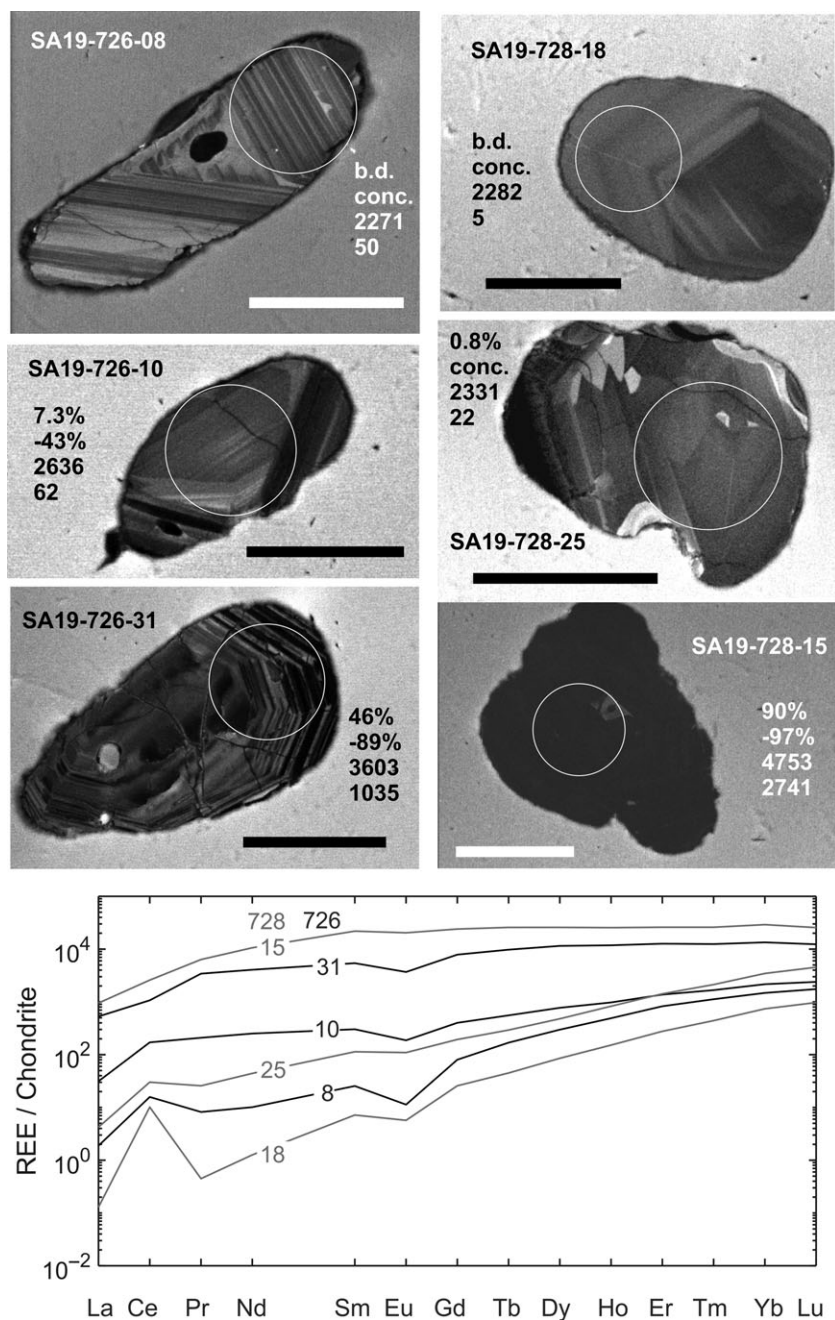


Fig. 5. CL photomicrographs of selected zircon grains from samples SA19-726 and SA19-728, with chondrite-normalized REE patterns. See Figure 3 for abbreviations.

(Dy/Sm) + (Dy/Nd) (Fig. 10b). For (Dy/Sm) + (Dy/Nd) > 8, there are only few grains with Th/U > 1, up to a maximum value of c. 2.5. In contrast, a significant number of grains with lower (Dy/Sm) + (Dy/Nd) have higher Th/U ratios, ranging to 3 and above.

Grains showing (Dy/Sm) + (Dy/Nd) > 8 have REE concentrations in the lower part of the overall range (Fig. 11), and these grains do not show any of the anomalous features with flat middle to heavy REE patterns, maxima in the middle REE range, and at least traces of positive Ce and negative Eu anomalies. The REE distributions of these grains are likely to reflect the composition of a magmatic protosource rock. In contrast, grains with (Dy/Sm) + (Dy/Nd) < 8 have high REE concentrations (up to $> 4 \times 10^4$ chondrites in the heavy to middle REE range) and anomalous distribution patterns (see also Figs 3–5). REE patterns that are flat

in the Gd to Lu range, and even relatively depleted in heavy REEs, are well known from metamorphic zircon that has grown in the presence of garnet, but such zircon will generally have heavy REE levels of 100 times chondrite or less, with distinct, positive Ce and negative Eu anomalies, and depletion in La, Pr and Nd (e.g. Hoskin & Schaltegger, 2003; Whitehouse & Platt, 2003; Skublov *et al.* 2012; Johnson *et al.* 2015; Jiao *et al.* 2017). None of these features are seen in the present high-REE zircon. Partitioning of heavy and middle REE into xenotime during Palaeoproterozoic diagenesis or metamorphism (e.g. Rasmussen *et al.* 2011) may cause a flattening of the heavy REE pattern in coexisting zircon, but would also be expected to cause a depletion rather than the observed increase in middle to heavy REE concentrations.

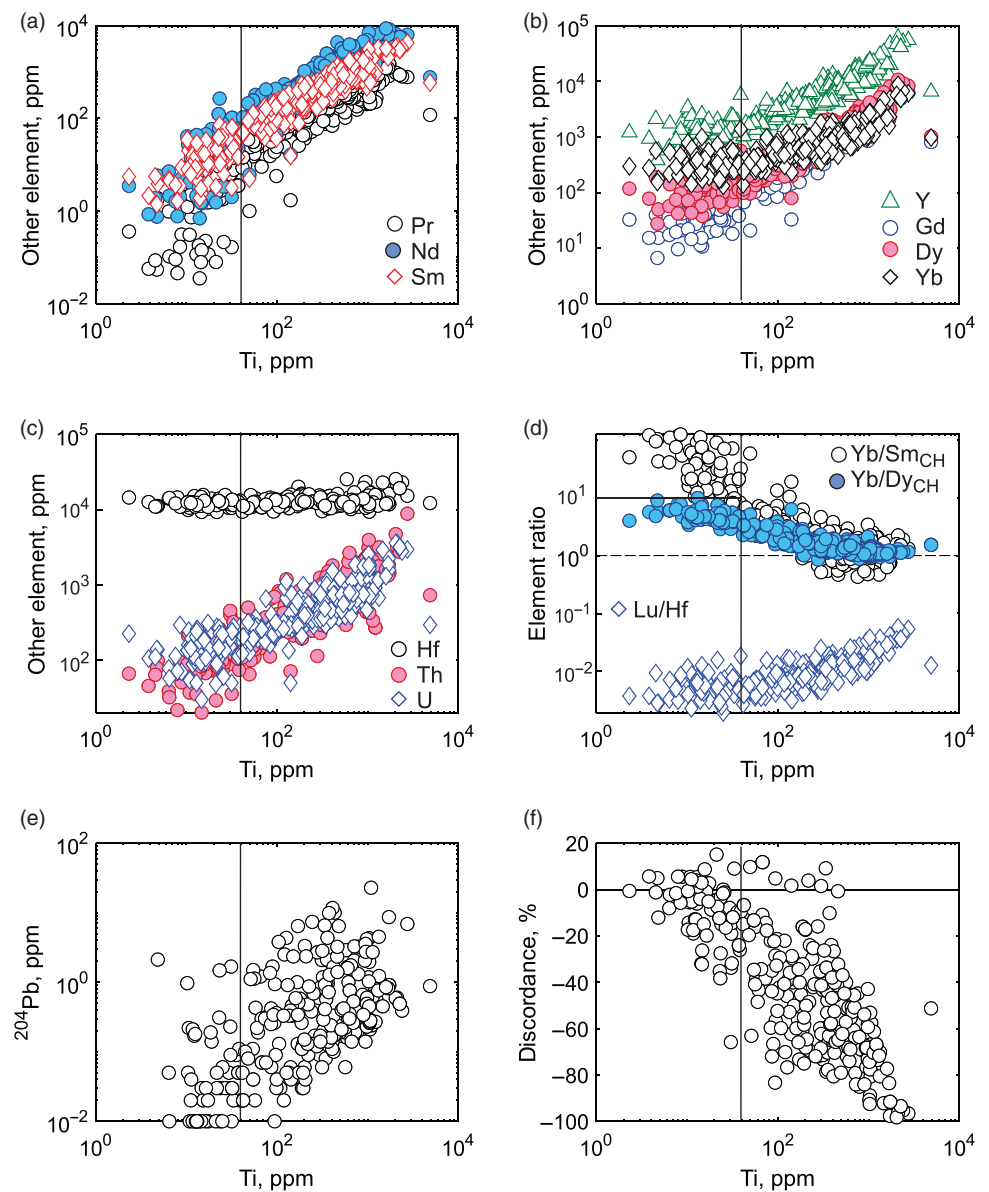


Fig. 6. (Colour online) Correlations with Ti of (a, b) REE Y; (c) Hf, Th and U; (d) chondrite-normalized Yb/Sm and Yb/Dy ratios (chondrite values from Boynton, 1984) and (d) Lu/Hf ratio; (e) ^{204}Pb (as proxy for common lead); and (f) U–Pb discordance.

6.b. The origin of U–Pb discordance: lead loss or uranium gain

Normal discordance in zircon can in principle have four different reasons: loss of radiogenic lead, gain of uranium, incorporation of common lead and accidental mixing of concordant domains of different ages. The last of these is an analytical artefact that can normally be avoided when using laser ablation inductively coupled plasma mass spectrometry (LA-ICP-MS) in time-resolved mode, and which will not be considered further. The present data have been corrected for common lead where required, so the third mechanism can also be disregarded, although the danger of correction-induced bias towards low ages exists, as discussed in Section 5.c. The preferred interpretation of normal discordance has always been loss of radiogenic lead, which may be induced by thermal overprint or interaction with fluids (e.g. Metzger & Krogstad, 1997; Geissler *et al.* 2003). Low-temperature weathering processes may induce loss of radiogenic lead from radiation-damaged zircon (Stern *et al.* 1966; Pidgeon *et al.* 2017). On the other hand, Pidgeon *et al.* (2017, 2019) found evidence of weathering-induced U–Pb discordance in

metamict zircon that must have been due to U introduction rather than to lead loss. At surface-near conditions, uranium is highly mobile as the uranyl ion (UO_2^{2+}) (Murphy & Shock, 1999). Hexavalent uranium can form its own minerals (e.g. uranyl phosphates, Dal Bo *et al.* 2016), and can be absorbed by metamict zircon or precipitate as secondary minerals along fractures in zircon (Pidgeon *et al.* 2017, 2019). If a concordant zircon with $^{207}\text{Pb}/^{206}\text{Pb}$ age t acquires D normal discordance in a recent process, the percentage discordance is given by

$$D\% = 100 \left(\frac{(^{206}\text{Pb}/^{238}\text{U})_{\text{observed}}}{e^{\lambda_8 t} - 1} - 1 \right) \quad (3)$$

where λ_8 is the decay constant of ^{238}U and $e^{\lambda_8 t} - 1$ is the $^{206}\text{Pb}/^{238}\text{U}$ ratio of a concordant zircon with age t . Since the change of the $^{206}\text{Pb}/^{238}\text{U}$ ratio can result from reduction of radiogenic lead content by a factor $x = ^{206}\text{Pb}_{\text{after}}/^{206}\text{Pb}_{\text{before}}$, or by an increase in the uranium concentration by a factor $y = ^{238}\text{U}_{\text{after}}/^{238}\text{U}_{\text{before}}$, a discordance of $D\%$ can be expressed by either

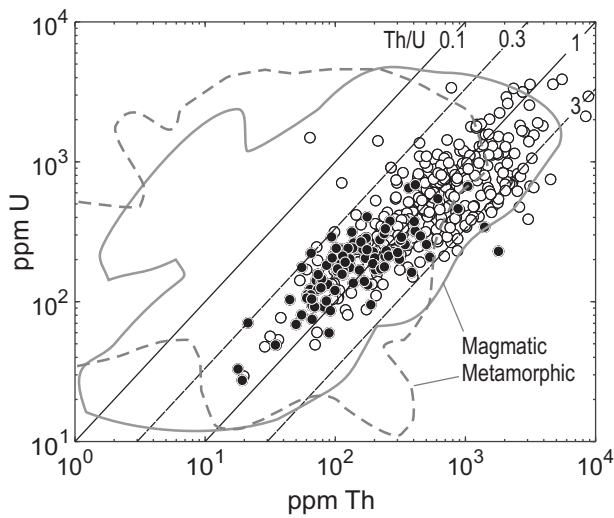


Fig. 7. Plot of U versus Th concentration of the detrital zircon in the present study, compared with lines of constant Th/U ratio, and fields of compiled data from zircon in magmatic and metamorphic rocks (data from Kirkland *et al.* 2015 and Yakymchuk *et al.* 2018, respectively). Filled circles: analyses with $^{206}\text{Pb}/^{204}\text{Pb} > 2000$.

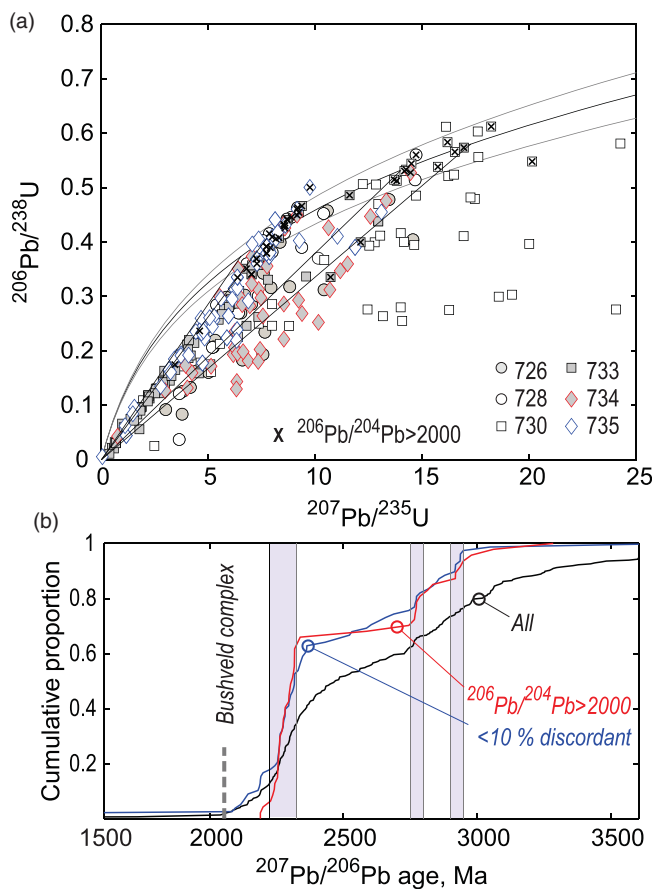


Fig. 8. (Colour online) (a) Concordia diagram showing common-lead-corrected analyses of 297 detrital zircon grains from the six samples. (b) Empirical, cumulative distribution curves constructed for the full dataset, and the data after two different data filtering methods (10% discordance and $^{206}\text{Pb}/^{204}\text{Pb} > 2000$). Shaded background represents three age fractions that can be discerned in the filtered data.

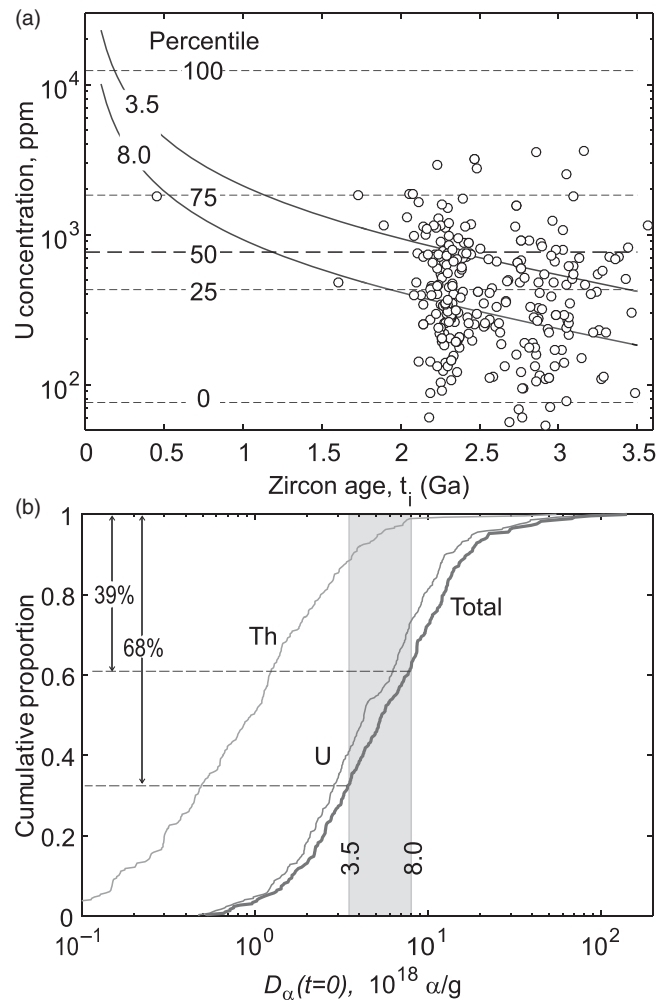


Fig. 9 (a) Uranium concentration of detrital zircon plotted against common-lead-corrected $^{207}\text{Pb}/^{206}\text{Pb}$ age. Broken, horizontal lines are percentile values for the uranium concentration of igneous zircon in granitic rocks, according to Belousova *et al.* (2002). The 0 percentile is the minimum, 100 percentile the maximum and 50 percentile the median. Contours of $D_{\alpha}(0)$ as a function of zircon age are shown for values of $3.5 \times 10^{18} \alpha/\text{g}$ and $8 \times 10^{18} \alpha/\text{g}$, corresponding to zircon that will be at the percolation point, and to those that are fully metamict at the present time. (b) The distribution of $D_{\alpha}(0)$ of the pooled set of detrital zircon in this study, calculated from Equation (1) using common-lead-corrected $^{207}\text{Pb}/^{206}\text{Pb}$ ages for t_1 and the observed U and Th concentrations. Note the concentration from U and its decay series significantly exceeds that of Th. A total of 68% of the zircon will have passed the percolation point, and 39% will be completely metamict.

$$D\% = 100(x - 1) \text{ or } D\% = 100(1/y - 1) \quad (4)$$

depending on which process is responsible. Although increases of uranium concentration by up to an order of magnitude in the most altered zircon grains are permitted by the present data (Fig. 10a), which can generate up to 90% of normal discordance, the inverse relationship between x and y makes uranium gain less efficient than lead loss to generate such high degrees of normal discordance. Most likely, both U gain and Pb loss have contributed to the discordance pattern of the detrital zircon studied here.

6.c. Conditions of alteration

The increase in concentration of any element in altered detrital zircon requires input of the element from some source external to the

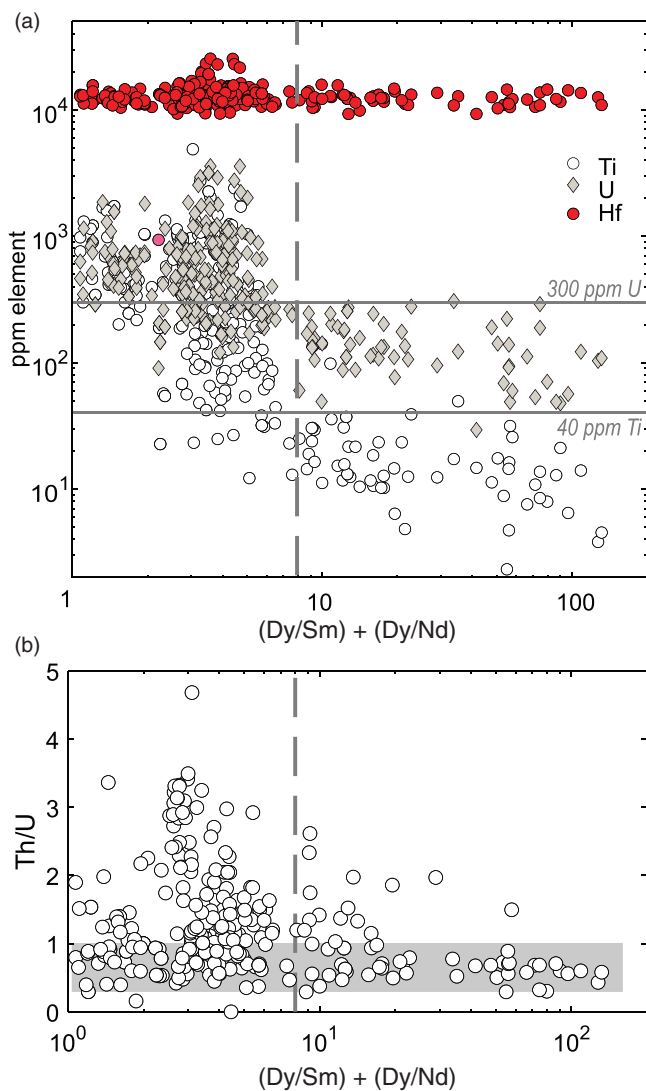


Fig. 10. (Colour online) (a) Variation of Ti, U and Hf concentration with the sum of un-normalized ratios $(Dy/Sm) + (Dy/Nd)$, proposed as an alteration index for zircon by Bell *et al.* (2019). See text for further explanation. (b) Variation of Th/U with $(Dy/Sm) + (Dy/Nd)$. The shaded field is limited by Th/U ratios of 0.3 and 1.0.

zircon itself. Titanium is a high-field-strength element that has low solubility in aqueous solutions under most low-pressure and -temperature conditions (van Baalen, 1993), and will tend to behave as a locally immobile element during weathering of detrital Ti-minerals such as titanite (Tilley & Eggleton, 2005). Inorganic ligands other than fluoride have negligible effect on titanium solubility at low temperature (van Baalen, 1993). Elevated fluorine concentration may be important in hydrothermal systems, but is unrealistic for most for near-surface weathering scenarios. On the other hand, titanium shows enhanced low-temperature solubility at low pH, and in the presence of organic ligands (Cornu *et al.* 1999). The excess Ti is likely to be absorbed into the amorphous, metamict zircon, or precipitated as poorly crystalline Ti- or Fe-Ti oxides or hydroxides along fractures, as was envisaged for other non-formula elements in low-temperature altered zircon by Pidgeon *et al.* (2019).

Th has generally been regarded as immobile in low-temperature aqueous fluids (e.g. Braun *et al.* 1992), but there is evidence for at least local remobilization of Th during weathering under hot and

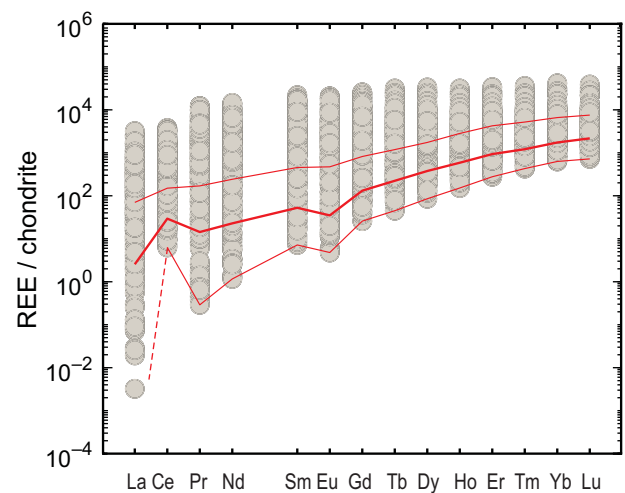


Fig. 11. (Colour online) Summary of chondrite-normalized REE patterns of the detrital zircon from the present study. To avoid clutter, the total variation is indicated by grey bars only (see Figs 3–5 for examples of actual patterns). The field of variation of detrital zircon with $(Dy/Sm) + (Dy/Nd) > 8$ is outlined by minimum, median and maximum lines. This group also shows a dominance of heavy over middle REEs as expected for magmatic zircon (e.g. Hoskin & Schaltegger, 2003). Chondrite concentrations according to Boynton (1984).

humid conditions (Braun *et al.* 2005; Du *et al.* 2012). At pH < 7, Th forms stable, soluble complexes with phosphate-, sulphate- and organic ligands, which enhances its solubility under acid conditions (Langmuir & Herman, 1980). Pidgeon *et al.* (2017, 2019) found that Th can indeed be introduced into radiation-damaged zircon during weathering, and that introduction of Th and U may be at least partly independent processes. This is also indicated by our data, with a general increase in Th/U seen in the more altered zircon, suggesting that Th is introduced to a greater extent than U.

During Late Cretaceous time, the bedrock below the African Surface was deeply weathered under hot, humid and acidic (pH c. 4) conditions (Partridge & Maud, 1987; Partridge, 1998; Partridge *et al.* 2006). These are conditions that would favour local mobility of Ti and Th. Weathering has continued to the present day, under variable temperature and humidity conditions. The increase in Ti seen in the altered zircon may be due to millimetre-to-centimetre-scale mobilization of Ti released by leaching of detrital titanite and ilmenite during deep weathering in periods of favourable climatic conditions during Cretaceous and Cenozoic time. The accompanying enrichment in light to middle REEs, Y, U and Th is most likely due to release by leaching of detrital apatite and possibly monazite in the same process.

6.d. Implications for detrital zircon geochronology

The U–Pb and trace-element characteristics of detrital zircon in the samples of Magaliesberg and Rayton formation analysed in this study are largely consequences of Cretaceous to recent alteration induced by weathering. Less than 20% of the grains analysed have retained a reliable memory of their protosource. A data-filtering routine based on a maximum level of common lead contamination removes noise from the ²⁰⁷Pb/²⁰⁶Pb age distribution, so that distinct age fractions can be identified. Alternative trace-element-based parameters may be used to filter data, using a minimum value for $(Dy/Sm) + (Dy/Nd)$ as suggested by Bell *et al.* (2019, but with a limit at 8 in the present data), $D_{\alpha}(0) < 3.5 \times 10^{18} \alpha/g$,

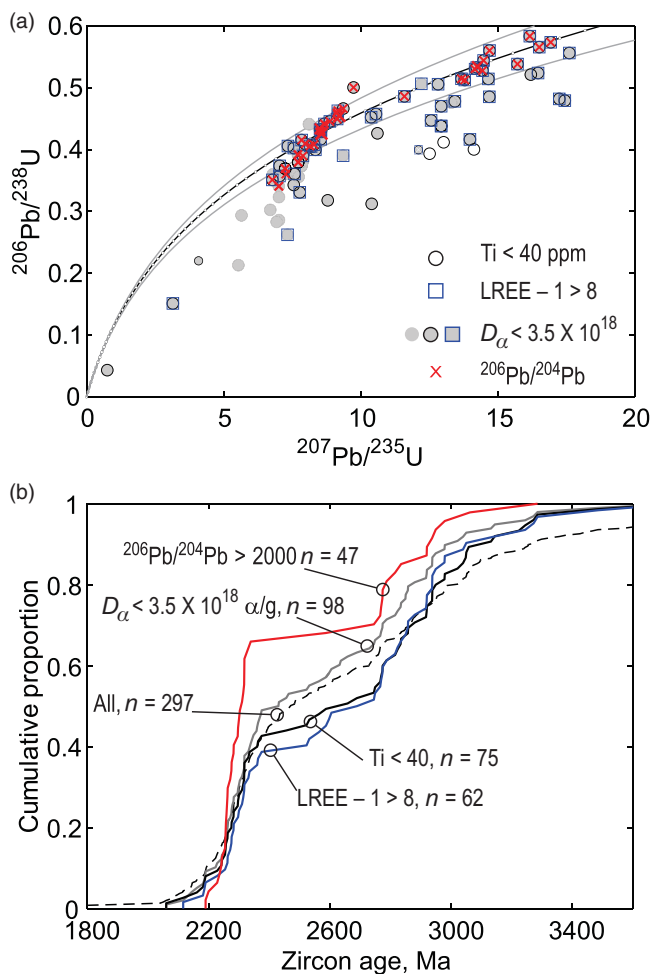


Fig. 12. (Colour online) Comparison of the effect of different data filters on the detrital zircon U–Pb data. (a) Concordia diagram including $\pm 10\%$ discordance contours. Only points that have passed the different data filters are shown; note that points that have passed more than one filter are shown by superimposed signatures. (b) Cumulative age distribution curves for $^{207}\text{Pb}/^{206}\text{Pb}$ ages, with filters and remaining point numbers as indicated.

or a maximum concentration limit for non-structural elements (e.g. $\text{Ti} \leq 40$ ppm). These routines will remove grains whose trace-element chemistry has been altered, but will still allow grains with disturbed U–Pb systematics to pass, and will not reveal the pattern of age fractions suggested by the $^{206}\text{Pb}/^{204}\text{Pb}$ filtered data (Fig. 12). However, it can be a viable screening for datasets where ^{204}Pb cannot be reported because of high mercury backgrounds during analysis.

As was pointed out by Pidgeon *et al.* (2017), the possibility that U has been introduced by late processes has the implication that the $D_\alpha(0)$ calculated from observed concentrations by Equation (1), and hence also the degree of metamictization estimated from Equation (2), may overestimate the real alpha dose and radiation damage of the crystal structure. Uranium added to an old zircon in Cenozoic time has only been able to induce minor radiation damage on top of what has been accumulated throughout the lifetime of the crystal at the lower, primary concentrations of the radioactive elements. If so, the calculated $D_\alpha(0)$ value would be less useful as a filtering criterion for detrital zircon data. Furthermore, calibration methods for LA-ICP-MS that use present-day U and Th concentrations or counting rates to

compensate for radiation damage of the crystal structure (e.g. Sliwinski *et al.* 2017) may overestimate damage and thus introduce bias. Some studies have found that the degree of radiation damage in zircon estimated from present-day U and Th concentrations exceeds the structural damage that can be measured by Raman spectroscopy, which is commonly interpreted as evidence for late annealing of the crystal structure, even where there is no other evidence of thermal overprint (e.g. Wang *et al.* 2014). This may instead be a consequence of overestimation of D_α due to late introduction of U and Th. Although perhaps of less importance for detrital zircon studies, it must be noted that weathering-related change in U and Th contents also invalidates the common Pb-correction routine described by Andersen (2002).

The problems outlined here affect detrital zircon in old sedimentary rocks that have been exposed to chemical weathering under climatic conditions that favour element mobility. This would apply to any Precambrian sandstone in areas undergoing tropical or sub-tropical weathering today, or which has been exposed to such weathering in the past. The present samples were taken from natural exposures and roadcuts. As long as weathering extends far below the natural surface (several tens of metres in part of South Africa; Partridge & Maud, 1987), surface or near-surface samples are less useful for detrital zircon geochronology than drillcore and mine samples from well below the weathered zone. Data from surface samples should therefore be interpreted with great care. Trace-element data may provide information on the extent of alteration, and should therefore be included in analytical protocols whenever possible, but may not provide a sufficiently effective data filter to remove the effects of late weathering.

Hf isotope data have not been considered in the present study. The most significant effect on time-corrected $^{176}\text{Hf}/^{177}\text{Hf}$ ratios or epsilon-Hf values is likely to be caused by shifts in the U–Pb age (Guitreau & Blichert-Toft, 2014). As a result of the elevated Hf concentration, and its apparent resistance to the late processes (Figs 6c, 10a), weathering is unlikely to affect the present-day $^{176}\text{Hf}/^{177}\text{Hf}$ ratio. However, the change in Lu/Hf ratio due to REE gain in the most severely affected zircon grains (Fig. 6d) suggests that time-corrected $^{176}\text{Hf}/^{177}\text{Hf}$ and epsilon-Hf(*t*) values may be modified, even when the true (i.e. protosource) age of the zircon can be estimated.

7. Conclusions

Sandstones and contact metamorphic quartzites belonging to the Magaliesberg and Rayton formations of the upper part of the Palaeoproterozoic Pretoria Group have been in a near-surface position since the Cretaceous Period, and exposed to chemical weathering under variable climatic conditions for 20–70 Ma. Whereas fully crystalline zircon has been able to survive such exposure without modification of its primary uranium–lead and trace-element characteristics, radiation-damaged zircon has been severely affected, causing increasing U–Pb discordance, increasing content of common lead and non-structural trace elements, and changing REE distribution patterns that are strongly enriched and flat to concave downwards in the middle to heavy REE range. U and Th concentrations were increased in the process, but the two elements are at least partly decoupled, resulting in a wide range of Th/U in zircon that has been affected. Late increases in U and Th have the additional consequence that the accumulated alpha dose that can be estimated from observed element concentrations is

likely to overestimate the real dose absorbed through the lifetime of the zircon.

Only c. 15% of the detrital grains in the samples analysed in this study have escaped severe disturbance of their U–Pb and trace-element system. The use of data filters to such detrital zircon datasets is necessary. This study suggests that the conventional, discordance-based data filter, and alternatives based on trace-element analyses, are not sufficiently effective. Filtering the analyses on $^{206}\text{Pb}/^{204}\text{Pb}$ ratio or common lead content prior to correction works better, but leads to severe reduction of the number of useful grains in the dataset.

To achieve qualitative representativity of detrital zircon data, random sampling of zircon grains is commonly accepted as being necessary. This has the consequence that analysis of radiation-damaged zircon cannot be avoided. The results of this study raise doubts about the applicability of data from randomly sampled grains in provenance analysis of ancient sedimentary successions that have been exposed to weathering under hot and humid conditions. An alternative approach using selective sampling and/or pre-treatment of the zircon separates has the consequence that qualitative representativity is sacrificed, also causing a risk of biased interpretations.

Supplementary material. To view supplementary material for this article, please visit <https://doi.org/10.1017/S001675682100114X>

Acknowledgements. This study has received support from the University of Johannesburg through a DVP grant to TA; from the Department of Geosciences, University of Oslo through the departmental “Småforsk” funding program; and from Orlaug Merkesdal’s foundation. We thank Dr Magnus Kristoffersen for support in the ICPMS laboratory, and Siri Simonsen for SEM-CL imaging. MAE acknowledges the NRF for IPRR grant 119297. We thank Dr Lily Jackson for editorial handling, and reviewers Dr Udo Zimmermann and Dr Elisabeth Bell for helpful comments.

Declaration of interest. None

References

- Alexandre P, Andreoli MAG, Jamison A and Gibson RL (2006) $^{40}\text{Ar}/^{39}\text{Ar}$ age constraints on low-grade metamorphism and cleavage development in the Transvaal Supergroup (central Kaapvaal craton, South Africa): implications for the tectonic setting of the Bushveld Igneous Complex. *South African Journal of Geology* **109**, 393–410.
- Andersen T (2002) Correction of common lead in U–Pb analyses that do not report ^{204}Pb . *Chemical Geology* **192**, 59–79.
- Andersen T, Elburg M and Magwaza B (2019a) Sources of bias in detrital zircon geochronology: discordance, concealed lead loss and common lead correction. *Earth-Science Reviews* **197**, 102899. doi:10.1016/j.earscirev.2019.102899.
- Andersen T, Elburg MA and Van Niekerk HS (2019b) Detrital zircon in sandstones from the Palaeoproterozoic Waterberg and Nylstroom basins, South Africa: provenance and recycling. *South African Journal of Geology* **122**, 79–96.
- Balan E, Neuville DR, Trocellier P, Fritsch E, Muller J-P and Calas G (2001) Metamictization and chemical durability of detrital zircon. *American Mineralogist* **86**, 1025–33.
- Barker OB, Brandl G, Callaghan CC, Erikson PG and van der Neut M (2006) The Soutpansberg and Waterberg groups and the Blouberg formation. In *The Geology of South Africa* (eds MR Johnson, CR Anhaeusser and RJ Thomas), pp. 301–18. The Geological Society of South Africa, Johannesburg/Council for Geoscience, Pretoria.
- Bell EA, Boehnke P, Barboni M and Harrison TM (2019) Tracking chemical alteration in magmatic zircon using rare earth element abundances. *Chemical Geology* **510**, 56–71.
- Bell EA, Boehnke P and Harrison TM (2016) Recovering the primary geochemistry of Jack Hills zircons through quantitative estimates of chemical alteration. *Geochimica et Cosmochimica Acta* **191**, 187–202.
- Belousova EA, Griffin WL, O’Reilly SY and Fisher NI (2002) Igneous zircon: trace element composition as an indicator of source rock type. *Contributions to Mineralogy and Petrology* **143**, 602–22.
- Beukes NJ, de Kock MO, Vorster C, Ravhura LG, Frei D, Gumsley AP and Harris C (2019) The age and country rock provenance of the Molopo Farms Complex: implications for Transvaal Supergroup correlation in southern Africa. *South African Journal of Geology* **122**, 39–56. doi: 10.25131/sajg.122.0003
- Bindeman IN, Schmitt AK, Lundstrom CC and Hervig RL (2018) Stability of zircon and its isotopic ratios in high-temperature fluids: Long-term (4 months) isotope exchange experiment at 850°C and 50 MPa. *Frontiers in Earth Science* **6**, Article 59, doi: 10.3389/feart.2018.00059
- Black LP (1987) Recent Pb loss in zircon: a natural or laboratory-induced phenomenon? *Chemical Geology (Isotope Geoscience Section)* **65**, 25–33.
- Boynnton WV (1984) Cosmochemistry of the rare earth elements; meteorite studies. In *Rare Earth Element Geochemistry* (ed. P Henderson), pp. 63–114. Amsterdam: Elsevier Science Publishing Co.
- Braun J-J, Ngoupayou JRN, Viers J, Dupre B, Bedimo J-PB, Boeglin J-L, Robain H, Nyeck B, Freydier R, Nkamdjou LS, Rouiller J and Muller J-P (2005) Present weathering rates in a humid tropical watershed: Nsimi, South Cameroon. *Geochimica et Cosmochimica Acta* **69**, 357–87.
- Braun J-J, Pagel M, Herbillon A and Rosin C (1992) Mobilization and redistribution of REEs and thorium in a syenitic lateritic profile: a mass balance study. *Geochimica et Cosmochimica Acta* **57**, 4419–34.
- Brink MC, Waanders FB and Bisschoff AA (1997) Vredefort: a model for the anatomy of an astrobleme *Tectonophysics* **270**, 83–114.
- Brink MC, Waanders FB, Bisschoff AA and Gay NC (2000) The Foch Trust – Potschefstroom Fault structural system, Vredefort, South Africa: a model for impact related tectonic movement over a pre-existing barrier. *Journal of African Earth Sciences* **30**, 99–117.
- Cawthorn RG, Eales HV, Walraven F, Uken R and Watkeys MK (2006) The Bushveld Complex. In *The Geology of South Africa* (eds MR Johnson, CR Anhaeusser and RJ Thomas), pp. 261–281. The Geological Society of South Africa, Johannesburg/Council for Geoscience, Pretoria.
- Corfu F, Hanchar JM, Hoskin PWO and Kinney P (2003) Atlas of zircon textures. *Reviews in Mineralogy and Geochemistry* **53**, 469–500.
- Cornu S, Lucas Y, Lebon E, Ambrosi JP, Luizão F, Rouiller J, Bonnay M and Neal C (1999) Evidence of titanium mobility in soil profiles, Manaus, central Amazonia. *Geoderma* **91**, 281–95.
- Dal Bo F, Hatert F, Mees F, Filippo S, Baijot M and Fontaine F (2016) Crystal structure of bassetite and saléite: new insight into autunite-group minerals. *European Journal of Mineralogy* **28**, 663–75.
- Dorland HC (2004) *Provenance Ages and Timing of Sedimentation of Selected Neoproterozoic and Palaeoproterozoic Successions on the Kaapvaal Craton*. Ph.D. thesis, Rand Afrikaans University, Johannesburg. Published thesis.
- Du X, Rate AW and Gee MAM (2012) Redistribution and mobilization of titanium, zirconium and thorium in an intensely weathered lateritic profile in Western Australia. *Chemical Geology* **330–332**, 101–15.
- Eriksson PG, Altermann W, Catuneanu O, van der Merwe R and Bumby AJ (2001) Major influences on the evolution of the 2.67–2.1 Ga Transvaal basin, Kaapvaal craton. *Sedimentary Geology* **141–142**, 205–31.
- Eriksson PG, Altermann W and Hartzler FJ (2006) The Transvaal Supergroup and its precursors. In *The Geology of South Africa* (eds MR Johnson, CR Anhaeusser and RJ Thomas), pp. 237–60. The Geological Society of South Africa, Johannesburg/Council for Geoscience, Pretoria.
- Ewing RC, Meldrum A, Wang L, Weber WJ and Corrales LR (2003) Radiation effects in zircon. *Reviews in Mineralogy and Geochemistry* **53**, 387–435.
- Geissler T, Schaltegger U and Tomaschek F (2003) Re-equilibration of zircon in aqueous fluids and melts. *Elements* **3**, 43–50.
- Griffin WL, Belousova EA, Shee SR, Pearson NJ and O’Reilly SY (2004) Archean crustal evolution in the northern Yilgarn Craton: U–Pb and Hf-isotope evidence from detrital zircons. *Precambrian Research* **131**, 231–82.
- Griffin WL, Powell WJ, Pearson N and O’Reilly SY (2008) GLITTER: Data reduction software for laser ablation ICP-MS. *Mineralogical Association of Canada Short Course Series* **40**, 204–7.

- Guitreau M and Blichert-Toft J** (2014) Implications of discordant U-Pb ages on Hf isotope studies. *Chemical Geology* **385**, 17–25.
- Gumsley AP, Chamberlain KR, Bleeker W, Söderlund U, de Kock MO, Larsson ER and Bekker A** (2017) Timing and tempo of the Great Oxidation Event. *Proceedings of the National Academy of Sciences of the USA* **114**, 1811–6. doi:10.1073/pnas.1608824114
- Hannah JL, Bekker A, Stein HJ, Markey RJ and Holland HD** (2004) Primitive Os and 2316 Ma age for marine shale: implications for Paleoproterozoic glacial events and the rise of atmospheric oxygen. *Earth Planet Science Letters* **225**, 43–52.
- Harris N, McMillan A, Holness M, Uken R, Watkeys M, Rodgers N and Fallick A** (2003) Melt generation and fluid flow in the thermal aureole of the Bushveld Complex. *Journal of Petrology* **44**, 1031–54.
- Hay DC and Dempster TJ** (2009) Zircon alteration, formation and preservation in sandstones. *Sedimentology* **56**, 2175–91.
- Heilimo E, Mikkola PO and Halla J** (2007) Age and petrology of the Kaapinsalmi sanukitoid intrusion in Suomussalmi, Eastern Finland. *Bulletin of the Geological Society of Finland* **79**, 117–25.
- Holland H and Gottfried D** (1955) The effect of nuclear radiation on the structure of zircon. *Acta Crystallographica* **9**, 291–300.
- Hoskin PWO and Schaltegger U** (2003) The composition of zircon and igneous and metamorphic petrogenesis. *Reviews in Mineralogy and Geochemistry* **53**, 27–62.
- Huhma H, Mänttari I, Peltonen P, Kontinen A, Halkoaho T, Hanski E, Hokkanen T, Hölttä P, Juopperi H, Konnunaho J, Layahe Y, Luukkonen E, Pietikäinen K, Pulkkinen A, Sorjonen-Ward P, Vaasjoki M and Whitehouse M** (2012) The age of the Archaean greenstone belts in Finland. Espoo: Geological Survey of Finland, Special Paper, 54, 74–175.
- Jiao S, Fitzsimons ICW and Guo J** (2017) Paleoproterozoic UHT metamorphism in the Daqingshan Terrane, North China Craton: new constraints from phase equilibria modeling and SIMS U-Pb zircon dating. *Precambrian Research* **303**, 208–27.
- Johnson MR, van Vuuren CJ, Visser JNJ, Cole DI, Wickens H de V, Christie ADM, Roberts DL and Brandl G** (2006) Sedimentary Rocks of the Karoo Supergroup. In *The Geology of South Africa* (eds MR Johnson, CR Anhaeusser and RJ Thomas), pp. 461–99. The Geological Society of South Africa, Johannesburg/Council for Geoscience, Pretoria.
- Johnson TE, Clark C, Taylor RJM, Santosh M and Collins AS** (2015) Prograde and retrograde growth of monazite in migmatites: an example from the Nagercoil Block, southern India. *Geoscience Frontiers* **6**, 373–87.
- Kamo SL, Reimold WU, Krogh TE and Colliston WP** (1996) A 2.023 Ga age for the Vredefort impact event and a first report of shock metamorphosed zircons in pseudotachylite breccias and granophyre. *Earth and Planetary Science Letters* **144**, 369–88.
- Kirkland CL, Smithies RH, Taylor RJM, Evans N and McDonald B** (2015) Zircon Th/U ratios in magmatic environs. *Lithos* **212–215**, 397–414.
- Krogh TE** (1982) Improved accuracy of U-Pb zircon ages by the creation of more concordant systems using an air abrasion technique. *Geochimica et Cosmochimica Acta* **46**, 637–49.
- Langmuir D and Herman JS** (1980) The mobility of thorium in natural waters at low temperature. *Geochimica et Cosmochimica Acta* **44**, 1753–66.
- Ludwig KR** (2012) *User's Manual for Isoplot/Excel 3.75: A Geochronological Toolkit for Microsoft Excel*. Berkeley: Berkeley Geochronology Center, Special Publication no. 5, 75 pp.
- Mapeo RBM, Armstrong RA, Kampunzu AB, Modisi MP, Ramokate LV and Modie BNJ** (2006) A ca. 200Ma hiatus between the Lower and Upper Transvaal Groups of southern Africa: SHRIMP U-Pb detrital zircon evidence from the Segwagwa Group, Botswana: Implications for Palaeoproterozoic glaciations. *Earth and Planetary Science Letters* **244**, 113–32.
- Markwitz V and Kirkland CL** (2018) Source to sink zircon grain shape: constraints on selective preservation and significance for Western Australian Proterozoic basin provenance. *Geoscience Frontiers* **9**, 415–30.
- Mattinson JM** (2005) Zircon U-Pb chemical abrasion (“CA-TIMS”) method: combined annealing and multi-step partial dissolution analysis for improved precision and accuracy of zircon ages. *Chemical Geology* **220**, 47–56.
- Metzger K and Krogstad EJ** (1997) Interpretation of discordant U-Pb zircon ages: An evaluation. *Journal of Metamorphic Geology* **15**, 127–40.
- Moore JM, Polteau S, Armstrong RA, Corfu F and Tsikos H** (2012) The age and correlation of the Postmasburg Group, southern Africa: constraints from detrital zircon grains. *Journal of African Earth Sciences* **64**, 9–19.
- Murphy WM and Shock EL** (1999) Environmental aqueous geochemistry of actinides. *Reviews in Mineralogy and Geochemistry* **38**, 221–53.
- Nasdala L, Reiners PW, Garver JI, Kennedy AK, Stern RA, Balan E and Wirth R** (2004) Incomplete retention of radiation damage in zircon from Sri Lanka. *American Mineralogist* **89**, 219–31.
- Nasdala L, Wenzel M, Vavra G, Irmer G, Wenzel T and Kober B** (2001) Metamictization of natural zircon: accumulation versus thermal annealing of radioactivity-induced damage. *Contributions to Mineralogy and Petrology* **141**, 125–144.
- Partridge TC** (1998) Of diamonds, dinosaurs and diastrophism: 150 million years of landscape evolution in southern Africa. *South African Journal of Geology* **101**, 167–84.
- Partridge TC, Botha GA and Haddon JG** (2006) Cenozoic deposits of the interior. In *The Geology of South Africa* (eds MR Johnson, CR Anhaeusser and RJ Thomas), pp. 585–604. Geological Society of South Africa, Johannesburg/Council for Geoscience, Pretoria.
- Partridge TC and Maud RR** (1987) Geomorphic evolution of southern Africa since the Mesozoic. *South African Journal of Geology* **90**, 179–208.
- Piazolo S, Belousova E, La Fontaine A, Corcoran C and Cairney JM** (2017) Trace element homogeneity from micron- to atomic scale: implication for the suitability of the zircon GJ-1 as a trace element reference material. *Chemical Geology* **456**, 10–8.
- Pidgeon RT, Nemchin AA and Cliff J** (2013) Interaction of weathering solutions with oxygen and U-Pb isotopic systems of radiation-damaged zircon from an Archean granite, Darling Range Batholith, Western Australia. *Contributions to Mineralogy and Petrology* **166**, 511–23.
- Pidgeon RT, Nemchin AA, Roberts MP, Whitehouse MJ and Belluci JJ** (2019) The accumulation of non-formula elements in zircons during weathering: ancient zircons from the Jack Hills, Western Australia. *Chemical Geology* **530**, 119310.
- Pidgeon RT, Nemchin AA and Whitehouse MJ** (2017) The effect of weathering on U-Th-Pb and oxygen isotope systems of ancient zircons from the Jack Hills, Western Australia. *Geochimica et Cosmochimica Acta* **197**, 142–66.
- Rasmussen B, Bekker A and Fletcher IR** (2013) Correlation of Paleoproterozoic glaciations based on U-Pb zircon ages for tuff beds in the Transvaal and Huronian Supergroups. *Earth and Planetary Science Letters* **382**, 173–80.
- Rasmussen B, Fletcher IR and Muhling JR** (2011) Response of xenotime to prograde metamorphism. *Contributions to Mineralogy and Petrology* **162**, 1259–77.
- Salje EKH** (2006) Elastic softening of zircon by radiation damage. *Applied Physics Letters* **89**, 131902.
- Salje EKH, Chronsch J and Ewing RC** (1999) Is “metamictization” of zircon a phase transition? *American Mineralogist* **84**, 1107–16.
- Schaltegger U, Schmitt AK and Horstwood MSA** (2015) U-Th-Pb zircon geochronology by ID-TIMS, SIMS, and laser ablation ICP-MS: recipes, interpretations, and opportunities. *Chemical Geology* **402**, 89–110.
- Schreiber UM and Eriksson PG** (1992) The sedimentology of the post-Magaliesberg formation of the Pretoria Group, Transvaal Sequence, in the eastern Transvaal. *South African Journal of Geology* **95**, 1–16.
- Schröder S, Beukes NJ and Armstrong RA** (2016) Detrital zircon constraints on the tectonostratigraphy of the Paleoproterozoic Pretoria Group, South Africa. *Precambrian Research* **278**, 362–93.
- Skublov SG, Berezin AV and Bereshnaya NG** (2012) General relations in the trace element composition of zircons from eclogites with implications for the age of eclogites in the Belomorian Mobile Belt. *Petrology* **20**, 427–49.
- Sliwinski JT, Guillong M, Liebske C, Dunkl I, von Quadt A and Bachmann O** (2017) Improved accuracy of LA-ICP-MS U-Pb ages of Cenozoic zircons by alpha dose correction. *Chemical Geology* **472**, 8–21.
- Stacey JS and Kramers JD** (1975) Approximation of terrestrial lead isotope evolution by a two-stage model. *Earth Planetary Science Letters* **26**, 207–21.

- Stern RA, Bodorkos S, Kamo S, Hickman AH and Corfu F** (2009) Measurement of SIMS instrumental mass fractionation of Pb isotopes during zircon dating. *Geostandards and Geoanalytical Research* **33**, 145–68.
- Stern TW, Goldich SS and Newell MF** (1966) Effects of weathering on the U–Pb ages of zircon from the Morton Gneiss, Minnesota. *Earth and Planetary Science Letters* **1**, 369–71.
- Therriault AM, Grieve RA and Reimold U** (1997) Original size of the Vredefort structure: implications for the geological evolution of the Witwatersrand Basin. *Meteoritics and Planetary Science* **32**, 71–7.
- Tilley DB and Eggleton RA** (2005) Titanite low-temperature alteration and Ti mobility. *Clays and Clay Minerals* **53**, 100–7.
- van Baalen MR** (1993) Titanium mobility in metamorphic systems: a review. *Chemical Geology* **110**, 233–49.
- Veevers JJ and Saeed A** (2007) Central Antarctic provenance of Permian sandstones in Dronning Maud Land and the Karoo Basin: integration of U–Pb age and T_{DM} ages and host-rock affinity from detrital zircons. *Sedimentary Geology* **202**, 653–76.
- Wabo H, Humbert F, de Kock MO, Belyanin G, Söderlund U, Maré LP and Beukes NJ** (2019) Constraining the chronology of the Mashishing Dykes from the Eastern Kaapvaal Craton in South Africa. In *Dyke Swarms of the World: A Modern Perspective* (eds RK Srivastava, RE Ernst and P Peng), pp. 215–61. Springer Geology, doi:10.1007/978-981-13-1666-1_6.
- Walraven F** (1997) *Geochronology of the Rooiberg Group, Transvaal Supergroup, South Africa*. Information Circular No. 316, Economic Geology Research Unit, University of the Witwatersrand, Johannesburg, South Africa, 21 pp.
- Wang X-L, Coble MA, Valley JW, Shu X-J, Kitajima K, Spicuzza MJ and Sun T** (2014) Influence of radiation damage on Late Jurassic zircon from southern China: evidence from in situ measurements of oxygen isotopes, laser Raman, U–Pb ages, and trace elements. *Chemical Geology* **389**, 122–36.
- Watson EB, Wark DA and Thomas JB** (2006) Crystallization thermometers for zircon and rutile. *Contributions to Mineralogy and Petrology* **151**, 413–33. doi: 10.1007/s00410-006-0068-5
- Whitehouse MJ and Platt JP** (2003) Dating high-grade metamorphism—constraints from rare-earth elements in zircon and garnet. *Contributions to Mineralogy and Petrology* **145**, 61–74.
- Wiedenbeck M, Allé P, Corfu F, Griffin WL, Meier M, Oberli F, Von Quadt A, Roddick JC and Spiegel W** (1995) Three natural zircon standards for U–Th–Pb, Lu–Hf, trace element and REE analysis. *Geostandards Newsletter* **19**, 1–23.
- Williams IS** (2001) Response of detrital zircon and monazite, and their U–Pb isotopic systems, to regional metamorphism and host-rock partial melting, Cooma Complex, southeastern Australia. *Australian Journal of Earth Sciences* **48**, 557–80.
- Willner AP, Sindern S, Metzger K, Ermolaeva T, Kramm U, Puchkov V and Kronz A** (2003) Typology and single grain U/Pb ages of detrital zircons from Proterozoic sandstones in the SW Urals (Russia): early time marks at the eastern margin of Baltica. *Precambrian Research* **124**, 1–29.
- Yakymchuk C, Kirkland CL and Clark C** (2018) Th/U ratios in metamorphic zircon. *Journal of Metamorphic Geology* **36**, 715–37.
- Zeh A, Ovtcharova M, Wilson AH and Schaltegger U** (2015) The Bushveld complex was emplaced and cooled in less than one million years – results of zirconology, and geotectonic implications. *Earth and Planetary Science Letters* **418**, 103–14.
- Zeh A, Wilson AH and Gerdes A** (2020) Zircon U–Pb–Hf isotope systematics of Transvaal Supergroup – Constraints for the geodynamic evolution of the Kaapvaal Craton and its hinterland between 2.65 and 2.06 Ga. *Precambrian Research* **345**, 105760. doi:10.1016/j.precamres.2020.105760
- Zeh A, Wilson AH and Ovtcharova M** (2016) Source and age of upper Transvaal Supergroup, South Africa: age–Hf isotope record of zircons in Magaliesberg quartzite and Dullstroom lava, and implications for Paleoproterozoic (2.5–2.0 Ga) continent reconstruction. *Precambrian Research* **278**, 1–21.
- Zhang M and Salje EKH** (2001) Infrared spectroscopic analysis of zircon: radiation damage and the metamict state. *Journal of Physics: Condensed Matter* **13**, 3057–71.
- Zhao L, Guo F, Fan W, Zhang Q, Wu Y, Li J and Yan W** (2016) Early Cretaceous potassic volcanic rocks in the Jiangnan Orogenic Belt, East China: crustal melting in response to subduction of the Pacific–Izanagi ridge? *Chemical Geology* **437**, 30–43.
- Zimmermann U** (2018) The provenance of selected Neoproterozoic to lower Paleozoic basin successions of Southwest Gondwana: a review and proposal for further research. In *Geology of Southwest Gondwana* (eds S Siegesmund, MAS Basei, P Oyhantcabal and S Oriolo), pp. 561–91. Springer International Publishing AG, Regional Geology Reviews.